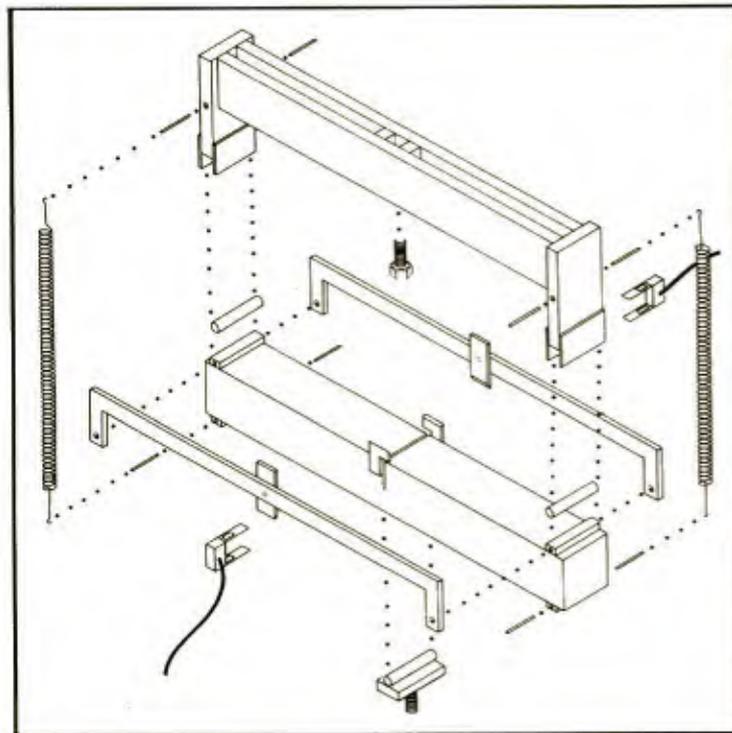# NCEL
Technical Report

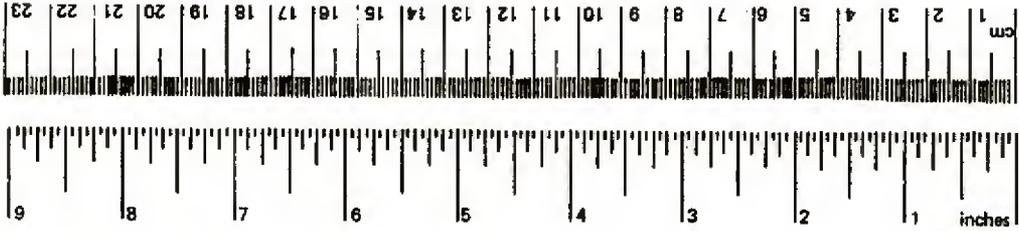# Fracture Energy for Three-Point Bend Tests on Single-Edge Notched Beams

ABSTRACT   Three test series of single-edge notched beams in three-point bending were conducted to evaluate the fracture energy of concrete. The fracture energy was determined from the area under the complete load versus load-point deflection diagram. The nonlinear Fictitious Crack Model was implemented in a finite element analysis, showing good agreement with the experimental data.

By varying the notch depth and the beam depth it was shown that the fracture energy, traditionally presented as a material property, depends upon the specimen size and configuration. This is attributed to the energy dissipation in the process zone which is not accounted for in the analytical model.

NAVAL CIVIL ENGINEERING LABORATORY   PORT HUENEME, CALIFORNIA 93043

METRIC CONVERSION FACTORS

Approximate Conversions to Metric Measures

Symbol	When You Know	Multiply by	To Find	Symbol
		LENGTH		
in	inches	*2.5	centimeters	cm
ft	feet	30	centimeters	cm
yd	yards	0.9	meters	m
mi	miles	1.6	kilometers	km
		AREA		
in²	square inches	6.5	square centimeters	cm²
ft²	square feet	0.09	square meters	m²
yd²	square yards	0.8	square meters	m²
mi²	square miles	2.6	square kilometers	km²
	acres	0.4	hectares	ha
		MASS (weight)		
oz	ounces	28	grams	g
lb	pounds	0.45	kilograms	kg
	short tons (2,000 lb)	0.9	tonnes	t
		VOLUME		
tsp	teaspoons	5	milliliters	ml
Tbsp	tablespoons	15	milliliters	ml
fl oz	fluid ounces	30	milliliters	ml
c	cups	0.24	liters	l
pt	pints	0.47	liters	l
qt	quarts	0.95	liters	l
gal	gallons	3.8	liters	l
ft³	cubic feet	0.03	cubic meters	m³
yd³	cubic yards	0.76	cubic meters	m³
		TEMPERATURE (exact)		
°F	Fahrenheit temperature	5/9 (after subtracting 32)	Celsius temperature	°C

*1 in = 2.54 (exactly). For other exact conversions and more detailed tables, see NBS Misc. Publ. 286, Units of Weights and Measures, Price $2.25, SD Catalog No. C13.10:286.

Approximate Conversions from Metric Measures

Symbol	When You Know	Multiply by	To Find	Symbol
		LENGTH		
mm	millimeters	0.04	inches	in
cm	centimeters	0.4	inches	in
m	meters	3.3	feet	ft
m	meters	1.1	yards	yd
km	kilometers	0.6	miles	mi
		AREA		
cm²	square centimeters	0.16	square inches	in²
m²	square meters	1.2	square yards	yd²
km²	square kilometers	0.4	square miles	mi²
ha	hectares (10,000 m²)	2.5	acres	
		MASS (weight)		
g	grams	0.035	ounces	oz
kg	kilograms	2.2	pounds	lb
t	tonnes (1,000 kg)	1.1	short tons	
		VOLUME		
ml	milliliters	0.03	fluid ounces	fl oz
l	liters	2.1	pints	pt
l	liters	1.06	quarts	qt
l	liters	0.26	gallons	gal
m³	cubic meters	35	cubic feet	ft³
m³	cubic meters	1.3	cubic yards	yd³
		TEMPERATURE (exact)		
°C	Celsius temperature	9/5 (then add 32)	Fahrenheit temperature	°F

°F   -40   0   32   80   98.6   120 160   200 212 °F
°C   -40 -20   0   20   37   40   60   80   100 °C

REPORT DOCUMENTATION PAGE		READ INSTRUCTIONS BEFORE COMPLETING FORM
1. REPORT NUMBER TR-924	2 GOVT ACCESSION NO. DN665019	3. RECIPIENT'S CATALOG NUMBER
4. TITLE (and Subtitle) FRACTURE ENERGY FOR THREE-POINT BEND TESTS ON SINGLE-EDGE NOTCHED BEAMS		5 TYPE OF REPORT & PERIOD COVERED Not Final; Oct 1986-Sep 1987
		6 PERFORMING ORG. REPORT NUMBER
7. AUTHOR(s) L. J. Malvar and G. E. Warren		8. CONTRACT OR GRANT NUMBER(s)
9. PERFORMING ORGANIZATION NAME AND ADDRESS NAVAL CIVIL ENGINEERING LABORATORY Port Hueneme, California 93043-5003		10. PROGRAM ELEMENT, PROJECT, TASK AREA & WORK UNIT NUMBERS 61153N; YR023-03-01-009
11. CONTROLLING OFFICE NAME AND ADDRESS NAVAL FACILITIES ENGINEERING COMMAND Alexandria, VA 22332		12. REPORT DATE March 1988
		13. NUMBER OF PAGES 28
14. MONITORING AGENCY NAME & ADDRESS(if different from Controlling Office)		15. SECURITY CLASS. (of this report) Unclassified
		15a. DECLASSIFICATION/DOWNGRADING SCHEDULE

16. DISTRIBUTION STATEMENT (of this Report)

Approved for public release; distribution unlimited.

17. DISTRIBUTION STATEMENT (of the abstract entered in Block 20, if different from Report)

18. SUPPLEMENTARY NOTES

19. KEY WORDS (Continue on reverse side if necessary and identify by block number)

Concrete, fracture mechanics, fracture energy, three-point bend beam, fictitious crack model

20. ABSTRACT (Continue on reverse side if necessary and identify by block number)

Three test series of single-edge notched beams in three-point bending were conducted to evaluate the fracture energy of concrete. The fracture energy was determined from the area under the complete load versus load-point deflection diagram. The nonlinear Fictitious Crack Model was implemented in a finite element analysis, showing good agreement with the experimental data

Continued

DD FORM 1473 EDITION OF 1 NOV 65 IS OBSOLETE
1 JAN 73

20. Continued

By varying the notch depth and the beam depth it was shown that the fracture energy, traditionally presented as a material property, depends upon the specimen size and configuration. This is attributed to the energy dissipation in the process zone which is not accounted for in the analytical model.

Library Card

Naval Civil Engineering Laboratory
FRACTURE ENERGY FOR THREE-POINT BEND TESTS ON
SINGLE-EDGE NOTCHED BEAMS, (Not Final), by
L.J. Malvar and G.E. Warren
TR-924   28 pp illus   Mar 1988   Unclassified

1. Fictitious Crack Model   2. Concrete   I. YR023-03-01-009

Three test series of single-edge notched beams in three-point bending were conducted to evaluate the fracture energy of concrete. The fracture energy was determined from the area under the complete load versus load-point deflection diagram. The nonlinear Fictitious Crack Model was implemented in a finite element analysis, showing good agreement with the experimental data.

By varying the notch depth and the beam depth it was shown that the fracture energy, traditionally presented as a material property, depends upon the specimen size and configuration. This is attributed to the energy dissipation in the process zone which is not accounted for in the analytical model.

CONTENTS

INTRODUCTION

Classical linear elastic fracture mechanics (LEFM), which has been successfully applied to metallic and brittle materials, is limited when applied to concrete. LEFM cannot model the behavior of small specimens of the size typically used in laboratories. As a consequence, several nonlinear models have been developed which approximate LEFM for large sizes. The two best known models are the fictitious crack model (FCM) introduced by Hillerborg et al. (Ref 1), and the smeared or crack band model (CBM) introduced by Rashid and developed by Bazant et al. (Ref 2, 3, 4, 5). Among others, the two-parameter model by Jenq and Shah (Ref 6) is more recent and is supported by only limited data.

In finite element applications, CBM approach shows a dependency on the element size used in the mesh. Results do not converge in successive analyses where the element size is continuously reduced. This problem can be circumvented by linking the softening stiffness of the cracked elements to the fracture energy G_f. However, G_f determined from the load-deflection diagram is suspected to depend on specimen geometry and size (Ref 5). The FCM is also based on G_f, which is assumed to be a material property.

The existing approaches for determination of the fracture energy are evaluated in this report and a new test method proposed. Three series of tests and a finite element analysis using FCM were conducted. The objectives were:

- Calculate the fracture energy following RILEM Technical Committee 50-FMC guidelines (Ref 7) and compare it to the fracture energy, G_f^*, according to a method presented in this report.

1

- Conduct a finite element analysis with different strain softening relations based on the experimental value of G_f.

- Determine the effect of notch-to-depth ratio and specimen size on G_f.

EVALUATION OF THE FRACTURE ENERGY G_f

For a beam in three-point bending (Figure 1a), the load typically varies with load-point deflection (LLPD) as shown in Figure 1b.

The LLPD plot comprises three stages of behavior. The deflection increases linearly with the load in the first stage and the crack is opened but does not extend. A fracture process zone develops during the second stage where microcracks form and slow crack growth is apparent. In the third stage, known as the strain softening zone, rapid crack growth is evident. During strain softening most of the damage to the specimen is concentrated in a narrow zone. This concentration is higher as the load carrying capacity decreases and energy dissipation eventually occurs through a single major crack. Strain softening has been considered a material characteristic.

The area, U_o, under the LLPD curve (Figure 2a) represents the energy required to break the specimen. For a single-edge notched beam in three-point bending, RILEM TC 50-FMC defined the fracture energy, G_f, as:

$$G_f = (U_o + mgd_o)/A$$

where A = ligament area = $B(W-a_o)$

B = width

W = specimen depth

a_o = notch depth

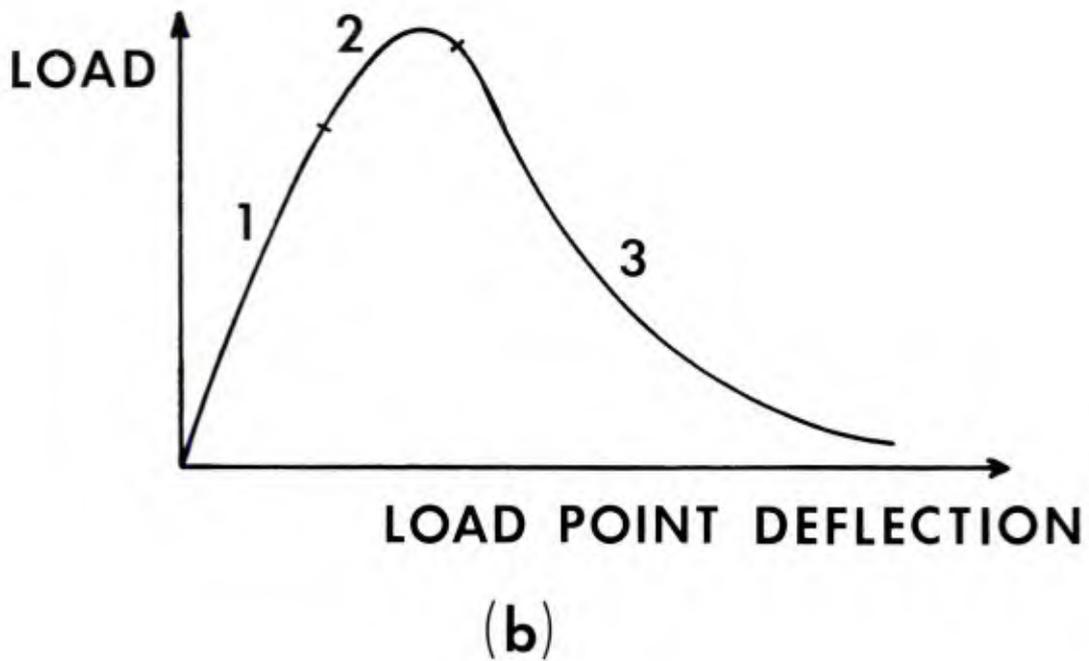mg = weight of the specimen

d_o = load-point deflection at fracture

2
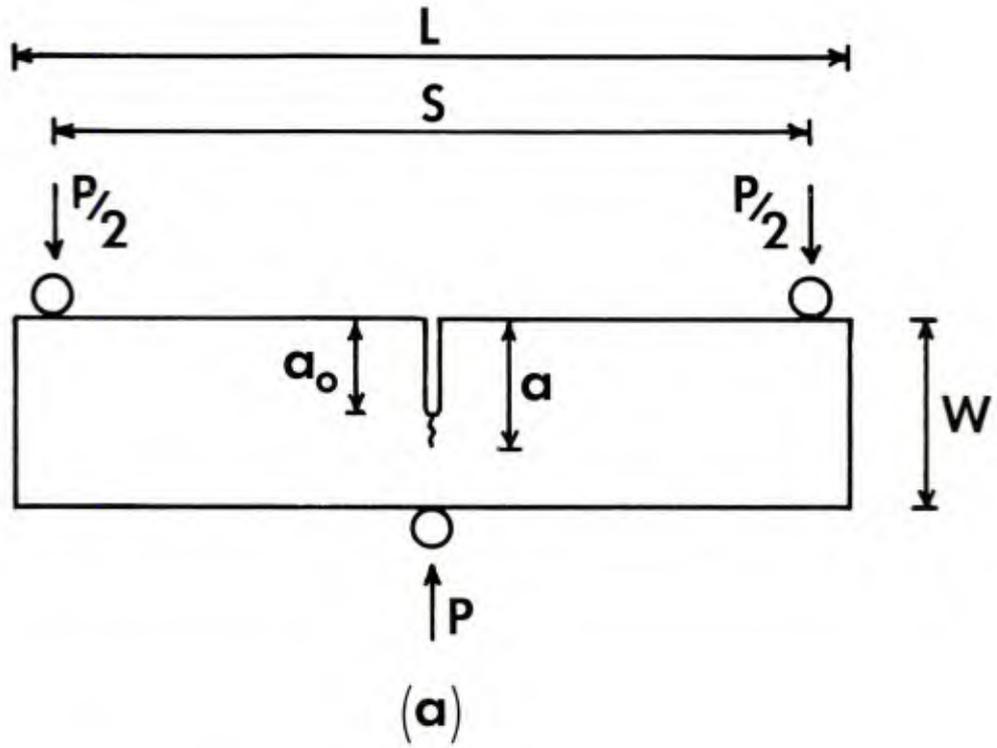
Figure 1. Specimen schematic and load versus load-point deflection plot.

$$G_f = \frac{U_o}{B\,(W - a_o)}$$
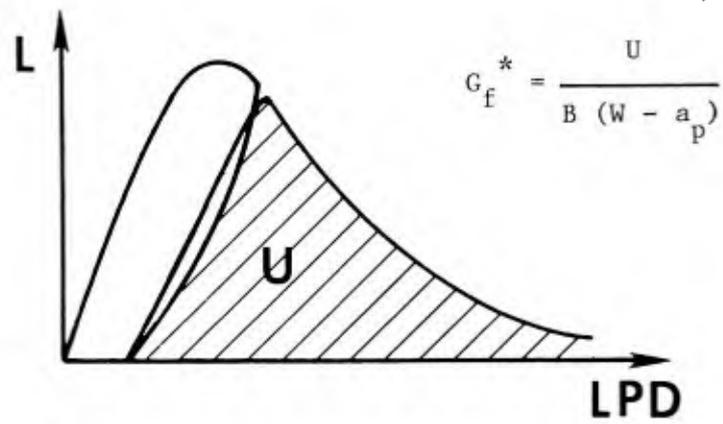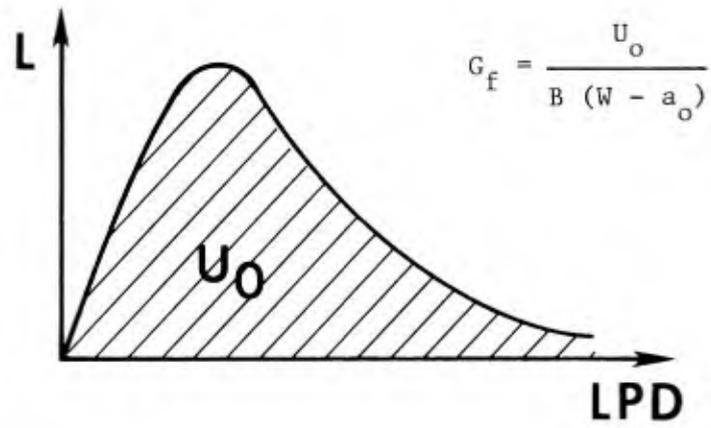
$$G_f^* = \frac{U}{B\,(W - a_p)}$$

Figure 2. Evaluation of the fracture energy.

This definition relies on the assumption that all the energy required to break the specimen is transformed into surface energy by extension of a single macrocrack. However, energy dissipation outside of the fracture zone is included in the determination of G_f and should not be overlooked. This energy depends on the specimen size and notch depth. It is dissipated in creating and extending a process zone by debonding aggregates and opening microcracks. Most of this energy consumption is believed to occur during slow crack growth. Consequently, using the whole area under the curve leads to an overestimate of G_f.

TEST METHOD

From the preceding observations it was concluded that an improved measure of the toughness of concrete would be obtained with a three-point bend beam specimen and the following procedure:

1. Set up the beam with the notch on the top surface. This will help in applying dye into the cracked surface for determining crack growth.

2. Load the specimen up to the point of instability defined as the point past peak load where the load drops off to 95 percent of its maximum value, then remove the load completely. The area enclosed in this load-unload loop includes the energy spent on formation of a process zone, slow crack growth, and the inelastic energy spent outside of the crack zone.

3. Insert dye through the notch and allow it to flow into the crack to highlight the crack length, a_p, at the point of instability.

4. Reapply the load and obtain the strain softening zone. A one-time unloading and reloading will not significantly affect the LLPD curve.

5

5. Define U as the total area under the LLPD curve minus the area in the load-unload loop indicated in the second step (see Figure 2b).

6. Define G_f^* as the energy spent on developing one major crack divided by the ligament area existing at that moment:

$$G_f^* = U/B(W-a_p)$$

DETAILS OF EXPERIMENTAL METHODOLOGY

Fracture Area

During the strain softening process a crack will actually follow a surface which is not flat but governed by the aggregate size and relative hardness compared to the mortar matrix. An invariant G_f will be obtained using the ligament area, $B(W-a_o)$, if the total energy spent in the formation of a unit projected area is constant (as assumed in the RILEM approach), or if the energy spent other than in formation of the macrocrack is discarded (as attempted here).

Precracking

Precracking of the specimen (or fatigue cracking) is not necessary in the proposed method. Measurement of the energy takes place only after a sharp crack has been formed, and does not depend on the initial condition, whether it is precracked, form notched, or saw notched.

Rate of Loading

RILEM recommends reaching peak load after 30 to 60 seconds which corresponds to a rate on the order of 5×10^{-6} m/sec (2×10^{-4} in./sec). The work of fracture and the strain energy release rate increase slightly (about 15 percent) for cross-head deflection rates from 5×10^{-7} to 5×10^{-5} m/sec (2×10^{-5} to 2×10^{-3} in./sec) (Ref 8).

6

Beam Weight

By supporting half of the beam weight at the ends, a complete LLPD curve is obtained. The LLPD curve actually begins after the applied load equals half of the specimen weight. In the LLPD plot the effect of beam weight is easily identified and discarded from the total area under the curve (Figure 6). This discarded area (1/2 weight x midspan deflection at total fracture) corresponds to work being transformed into potential energy as the center of gravity of the beam is forced up.

Displacement and Support Indentation

According to RILEM, the midspan deflection can be measured with reference to the loading apparatus as long as the inelastic indentations at the load points do not exceed 0.01 mm (0.0004 in.) (Ref 7). For nonstandard specimens with small span/depth ratios (e.g., S/W = 4) the inelastic indentations at the loading points are not negligible. They have to be considered or else the deflection due to load indentations has to be measured.

The error caused by inelastic indentation is estimated for a 27.65 MN/m^2 (4,000 psi) concrete specimen with dimensions 102 by 7 by 76 by 406 mm (4 by 3 by 16 in.) (depth by width by span), with an initial notch depth a_o = 25 mm (1 in.) and bearing directly on 51-mm (2-in.) diameter rollers. A maximum load of approximately 3.12 kN (700 lb) should be expected. The minimum bearing area at the center roller is 3.12/0.02765 = 113 mm^2 (0.175 in.^{2}) and the minimum bearing width is 113/76 = 1.5 mm (0.058 in.). This implies an indentation of the flat surface at the center roller only of 0.75 x 0.75/25.5 = 0.022 mm (about 0.001 in.). In this case the indentation represents about 25 percent of the midspan deflection at peak load.

The clip gage described by ASTM E399 seemed most appropriate for accurate displacement measurements. Clip gages were manufactured out of high strength aluminum (7075-T6) which was more readily available and easier to machine than a titanium alloy as recommended by ASTM. High strength aluminum presents a ratio of yield strength to modulus of

7

elasticity as high as 0.0069. High strength aluminum ensures a large range of measurement without permanent deformation of the gage. Two clip gages were employed, one on each side of the specimen, to mitigate errors due to asymmetry.

Point of Instability

The point of instability was chosen as the point after maximum load where the load decreases to 95 percent of its peak value as recommended by Swartz and Yap (Ref 9). A small variation of load near peak value is accompanied by a small displacement on the LLPD curve; however, this small amount of external work causes a significant crack advance. This is apparent on typical load versus crack mouth opening displacement (LCMOD) plots (Ref 9) where the CMOD increases significantly for almost constant maximum load. This instability is attributed to a redistribution of the elastic energy to surface energy inside the specimen. Thus, it is necessary to measure crack length past peak load to yield reliable and stable values.

TEST SETUP

The test setup is shown in Figures 3 and 4. Figure 5 is a photograph of an example specimen. Figure 3 shows the beams were tested with the notch on the top surface. The beam weight was supported by four springs aligned with reaction rollers. The rollers were located on bearing pads to minimize energy dissipation at the bearing points.

The load was applied through a closed-loop, servo-controlled, 20 kip, MTS testing machine. The tests were displacement controlled with a cross-head displacement rate of approximately 5.10^{-6} m/sec $(2.10^{-4}$ in./sec).
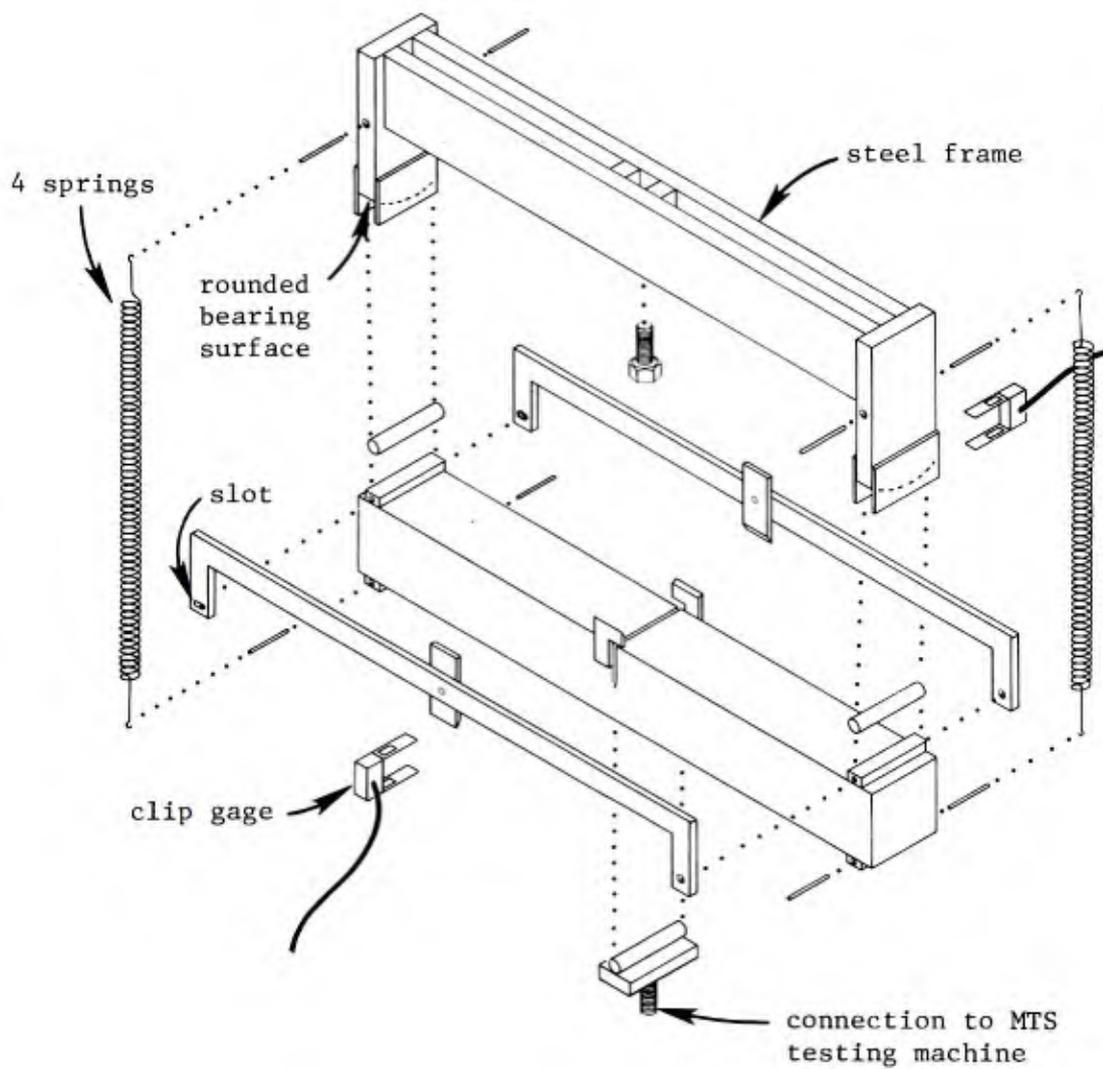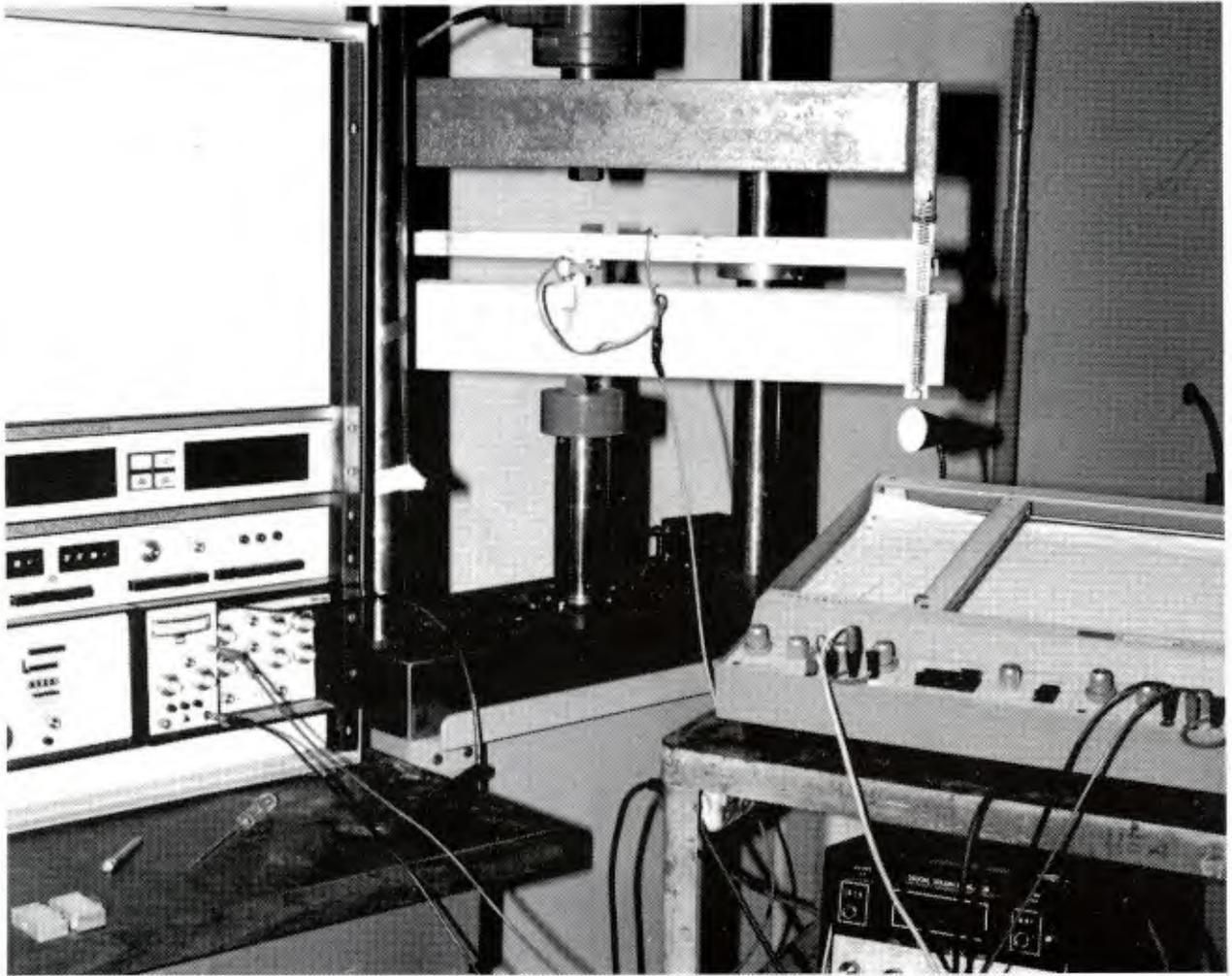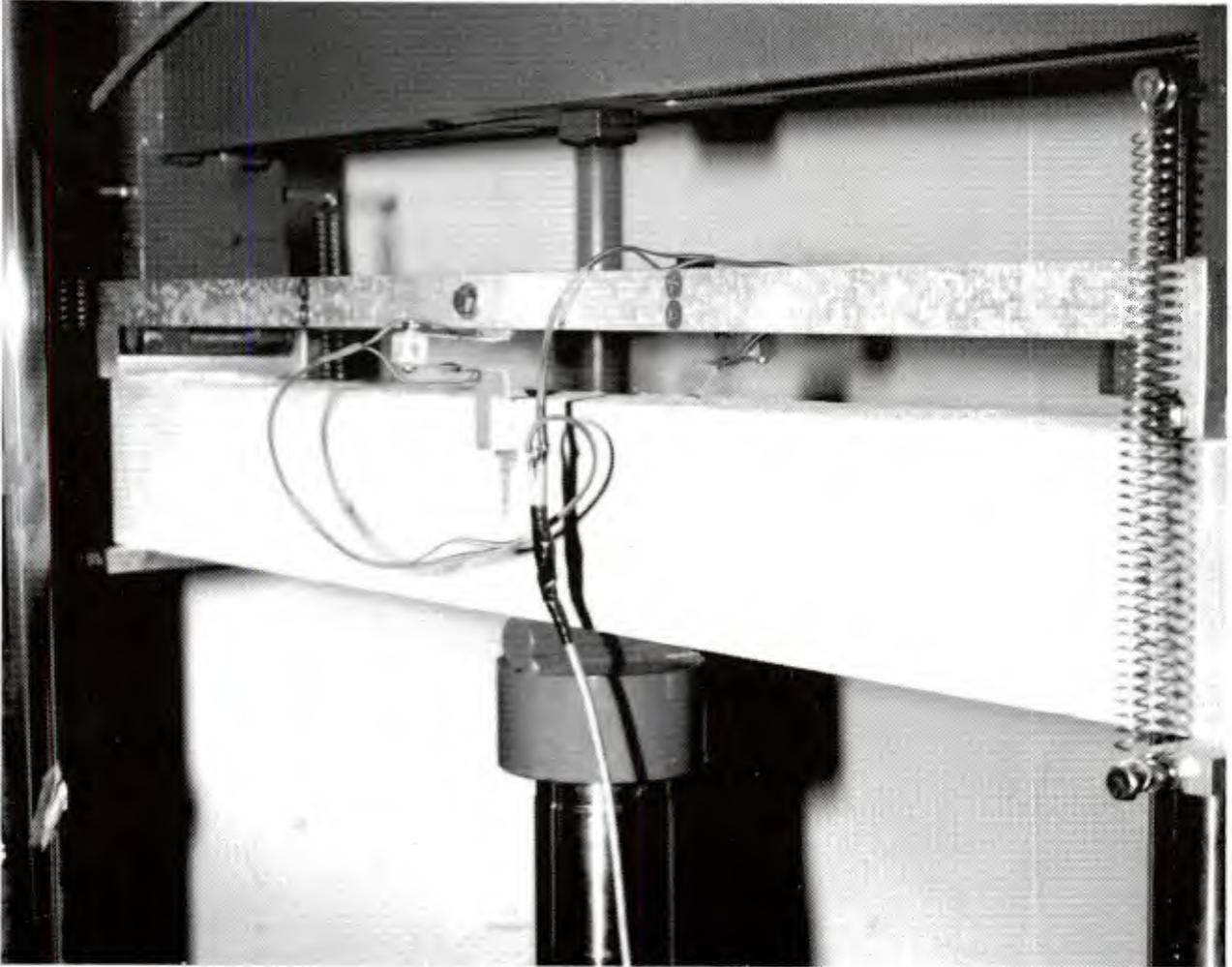
Figure 3. Set up schematic.

Figure 4.   Test setup.

Figure 5.   Clip gages and loading frame.

Two clip gages with a sensitivity of 0.0025 mm (0.0001 in.) were installed across from the load point. The clip gages bore against two aluminum beams which span across the reaction points (Figure 5). Tight fitting slots and holes machined in the frame allowed for rotation and horizontal displacement without vertical movement and negligible friction.

In order for the forces on the beam to be statically determinate, the two reaction rollers bore on a cylindrical surface whose axis was perpendicular to the rollers' axis. Thus, obtaining a single point of contact equivalent to spherical bearing.

An important advantage of the setup lies in obtaining the long tail of the LLPD plot (Figure 6), representing not only the beam weight but also other similar effects (such as clip gages weight and reaction) as well as possible constant friction. If some variable effects are present during the test, these can be evaluated by observing the linearity of the plot after the load carrying capacity of the beam has been spent.

TEST SERIES

Three series of tests were conducted. RILEM guidelines were followed in all tests for maximum aggregate size, conditions of storage, support and loading arrangement, accuracy of measurement, and rate of loading.

The concrete mixes with their mechanical properties are given in Table 1. The maximum aggregate size was 10 mm (3/8 in.) in all cases. The initial modulus of elasticity in compression, E, is also tabulated.

Series I

Twelve baseline beams (similar to RILEM's smallest specimen) were cast with dimensions of 102 by 102 by 788 by 838 mm (4 by 4 by 31 by 33 in.) (width by depth by span by length) (Figures 1 and 3). The notch-to-depth ratio, a_o/W, was 0.5. During the tests, the beams were

Table 1. Material Properties

Series	Cement (kg/m^3)	Water (kg/m^3)	M/C (%)	10 mm Gravel (kg/m^3)	Sand (kg/m^3)	f_c' (MPa)	f_t (MPa)	E (GPa)
I	279	167	0.60	1062	907	29.0	3.1	21.7
II	613	245	0.40	1034	443	58.9	4.2	24.5
III	400	220	0.55	1044	540	33.1	3.5	19.7

Notes:

The compressive strength, f_c', was obtained at 28, 35, and 30 days, respectively for each series. In every case, three 152- by 305-mm (6- by 12-in.) cylinders were tested.

The tensile strength, f_t, was obtained at 28, 32, and 29 days, respectively, using the same type of cylinders. Six splitting tensile tests were performed for Series I, then only three each for the other series due to the uniformity of the values.

The modulus of elasticity was calculated by measuring the cylinders strain at the beginning of the compression tests.

unloaded past peak load and both G_f and G_f^* obtained. The beams were tested in four groups of three after curing for 27, 28, 29, and 32 days in a fog room.

Series II

Twelve additional specimens with the same overall dimensions as Series I were prepared. They were divided into three groups of four beams with the same a_o/W. The initial notch-to-depth ratio was 0.3, 0.5, and 0.7 for groups 1, 2 and 3, respectively. In order to isolate the effect of notch depth from the effect of curing time one specimen of the four from each group was tested on the same day after curing for 28, 29, 32, and 33 days.
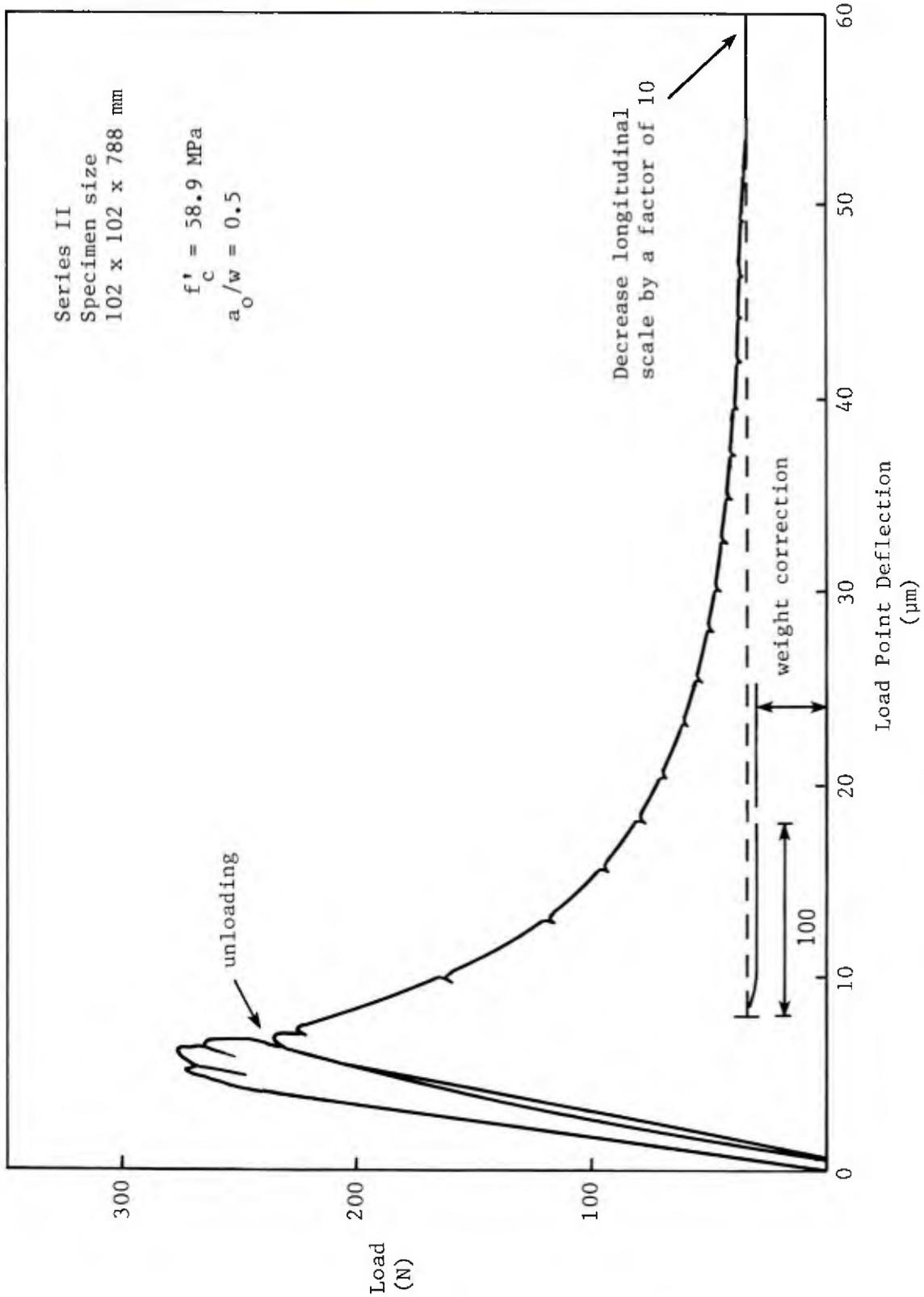
Figure 6. Load versus load-point deflection.

Series III

The third series consisted of four additional baseline specimens (same dimensions as series I with $a_o/W = 0.5$) plus four specimens with depths of 216 mm (8.5 in.) but with the same width, span, length, and a_o/W. While not geometrically similar to the standard RILEM specimen, the increase in ligament area (unbroken area at the notch) demonstrated the size effect on G_f.

One baseline specimen and one deeper beam were tested each day after curing for 28, 29, 30, and 32 days.

ANALYTICAL REPRESENTATION WITH FINITE ELEMENTS

The finite element program, ADINA (Ref 10) features user-supplied loading which can be expressed as an arbitrary function of nodal displacements. This allowed the implementation of an FCM approach. The element mesh was derived from Reference 11 and is shown in Figure 7. Due to symmetry, only half of a beam needed to be discretized. The notch-to-depth ratio, a_o/W, was chosen as 0.5. The beam was loaded in displacement control (both in the program and in the actual tests) and whenever the tensile strength, f_t, was reached at a node, the node was released and the midspan displacement was step increased until another f_t was exceeded at another node. This iterative process was continued until the crack progressed across the beam cross section.

The modulus of elasticity, E, used in the finite element analyses was measured as the initiation slope of the stress strain diagram of a compression test on a 152 - by 305-mm (6- by 12-in.) cylinder. Others, including Peterson (Ref 12), have used the dynamic modulus of elasticity, E_d, for analysis. The difference between dynamic and static is small (E_d is about 10 to 20 percent higher than E) and the loading rates between the cylinder tests and the three-point bend (3PB) tests is within one order of magnitude. Small differences have also been reported between tests carried out in tension compared to compression (around 10 percent lower according to Reference 13). Hence, E was chosen as the modulus of elasticity of the equivalent homogeneous elastic material.
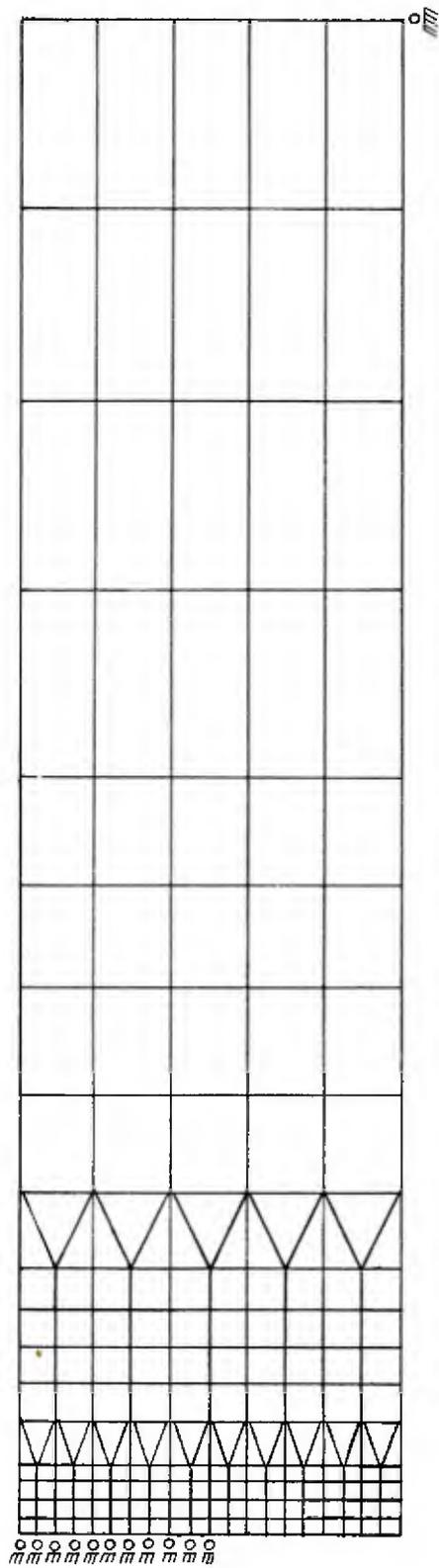
Figure 7. Finite element model.

Four stress versus crack width (σ versus w) relations were analyzed and are described in Figure 8. The straight line (SL) and bilinear or concrete (C) relations were proposed by Peterson (Ref 9), the exponential (E) relation is proposed by the authors (from curve fitting relationships derived in Ref 11 and 14), and the power function (P) by Reinhardt (Ref 15). In all cases, the relations conform to:

$$G_f = \int_0^\infty \sigma \, dw$$

as recommended by Hillerborg et al. (Ref 1).

RESULTS

Test Series I

Values of G_f^*, peak load, deflection at peak load (d_p), and deflection when the load carrying capacity of the beam vanishes (d_0), are reported in Table 2. The increase in crack length, Δa (measured by dye insertion) is also indicated. In some cases the closed loop servo control on the testing machine did not allow the unloading to take place immediately after the maximum load (when it decreases to about 95 percent of its peak value), so experimental values were not reported.

The LLPD plots were drawn until a long horizontal trace was obtained (Figure 6), indicating that the beam was not carrying any load. The noise and random friction then measured showed an effect of about ±4 N (±1 lb).

Dye insertion highlighted a crack front which appeared fairly straight. Typically the dye was inserted from the top, but in a couple of cases excess dye was allowed to run along the sides of the beam. In those cases the crack front appeared curved due to dye absorption on the sides.

17

Concrete C

$$\sigma = f_t \left(1 - 3\,\frac{w}{w_c}\right) \qquad \tfrac{1}{3} f_t < \sigma < f_t$$

$$\sigma = \tfrac{3}{7} f_t \left(1 - \frac{w}{w_c}\right) \qquad \sigma < \tfrac{1}{3} f_t$$

$$G_f = \tfrac{15}{54} f_t\, w_c$$

Power P

$$\sigma = f_t \left[1 - \left(\frac{w}{w_c}\right)^m\right]$$

$$G_f = \frac{m}{m+1} f_t\, w_c$$

Straight Line SL

$$\sigma = f_t \left(1 - \frac{w}{w_c}\right)$$

$$G_f = \tfrac{1}{2} f_t\, w_c$$

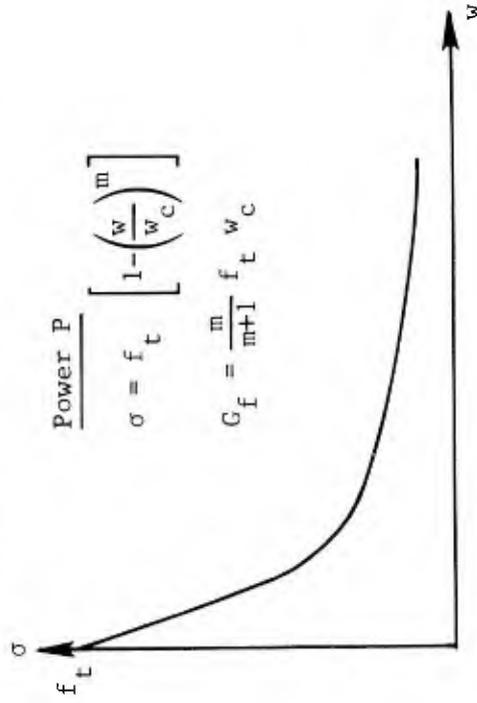## Exponential E
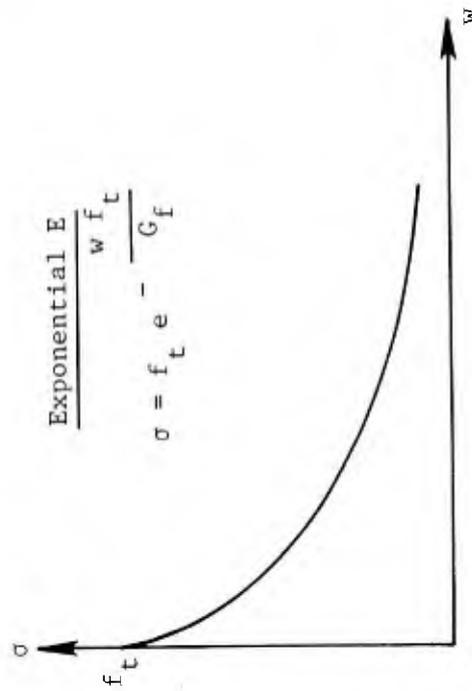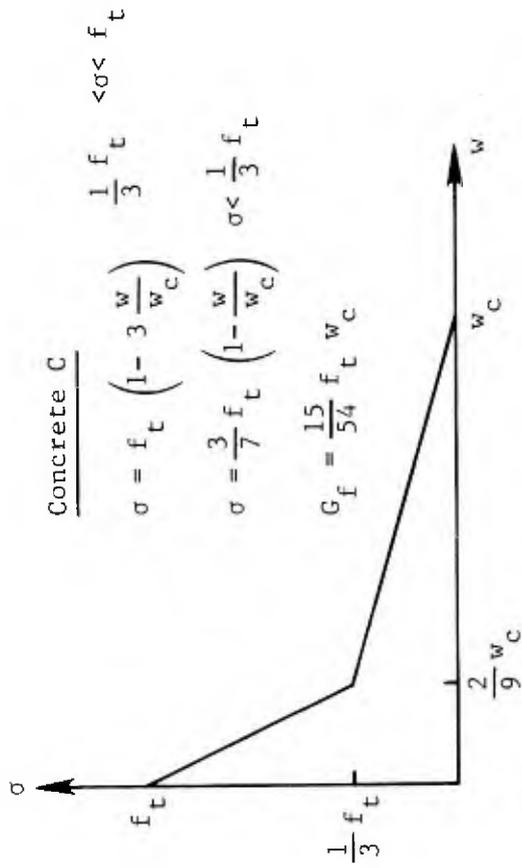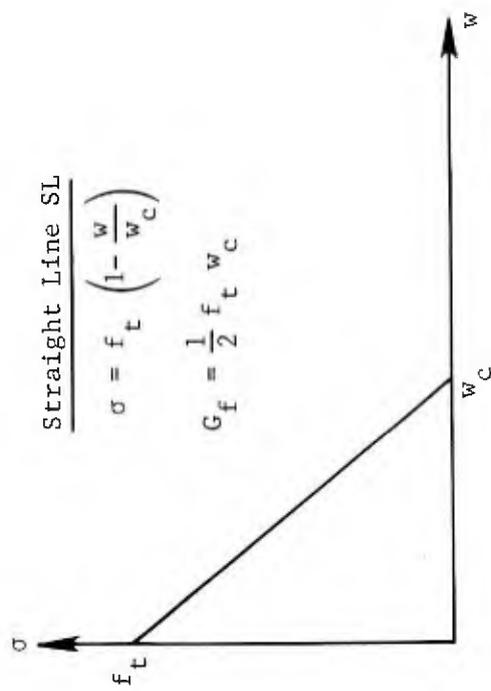
$$\sigma = f_t\, e^{-\dfrac{w\, f_t}{G_f}}$$

Figure 8. Stress versus crack width relations.

Table 2. Results – Series I

Specimen	G_f (M/m)	$G_f^{\#}$ (M/m)	Peak load (N)	Unloading at (% of peak load)	d_p (mm)	d_o (mm)	Δa (mm)
1	72.3	68.9	853	86	0.17	2.8	6.5
2	79.7	79.5	999	88	0.18	2.4	9.3
3	85.6	80.5	945	96	0.19	2.8	5.3
4	70.5	69.0	820	95	0.17	2.2	4.7
5	75.7	–	910	–	0.15	3.1	–
6	72.4	–	921	–	0.15	2.2	–
7	83.4	72.8	1011	91	0.16	2.5	3.0
8	75.3	69.6	950	88	0.17	2.9	5.9
9	68.1	63.6	883	87	0.13	2.4	5.7
10	68.6	–	950	–	0.16	2.6	–
11	84.1	–	950	–	0.16	2.7	–
12	79.8	76.4	997	94	0.15	2.0	3.6
Mean	76.3	72.5	932	90	0.16	2.6	5.5
Std Deviation	6.1	4.8					

19

Test Series II

Series II results are detailed in Table 3. A strong dependency of G_f on a_0/W is apparent with variations of about 25 percent (from its value at $a_0/W = 0.5$). G_f decreases as a_0/W increases. It should also be noted that G_f^* follows G_f closely.

Test Series III

Series III results are reported in Table 4. An increase in G_f of about 24 percent is observed when the depth is increased from 102 to 216 mm (4 to 8.5 in.).

Finite Element Analysis

Figure 9 shows the average LLPD plot from the 12 tests of Series I (solid trace) and the approximations from finite element analyses carried out using the four different σ versus w relations.

DISCUSSION

Effects on G_f

The variation of G_f with notch depth and beam depth indicates that the fracture energy is not a material property and is dependent on the specimen configuration. When modelling concrete as an equivalent homogeneous linear elastic material, all the energy supplied is assumed to be converted into surface energy by propagation of a single macrocrack. The microcracking in the process zone also dissipates energy that the model cannot take into account. The process zone depends upon the stress field which is dependent on the geometry (Ref 16). The process zone depends upon the aggregate-to-specimen size ratio which is a size parameter (Ref 4). This dependency raises a question about the reliability of using a specimen in three-point bending instead of in direct tension to determine the stress versus crack width relation.

20

Table 3. Results – Series II

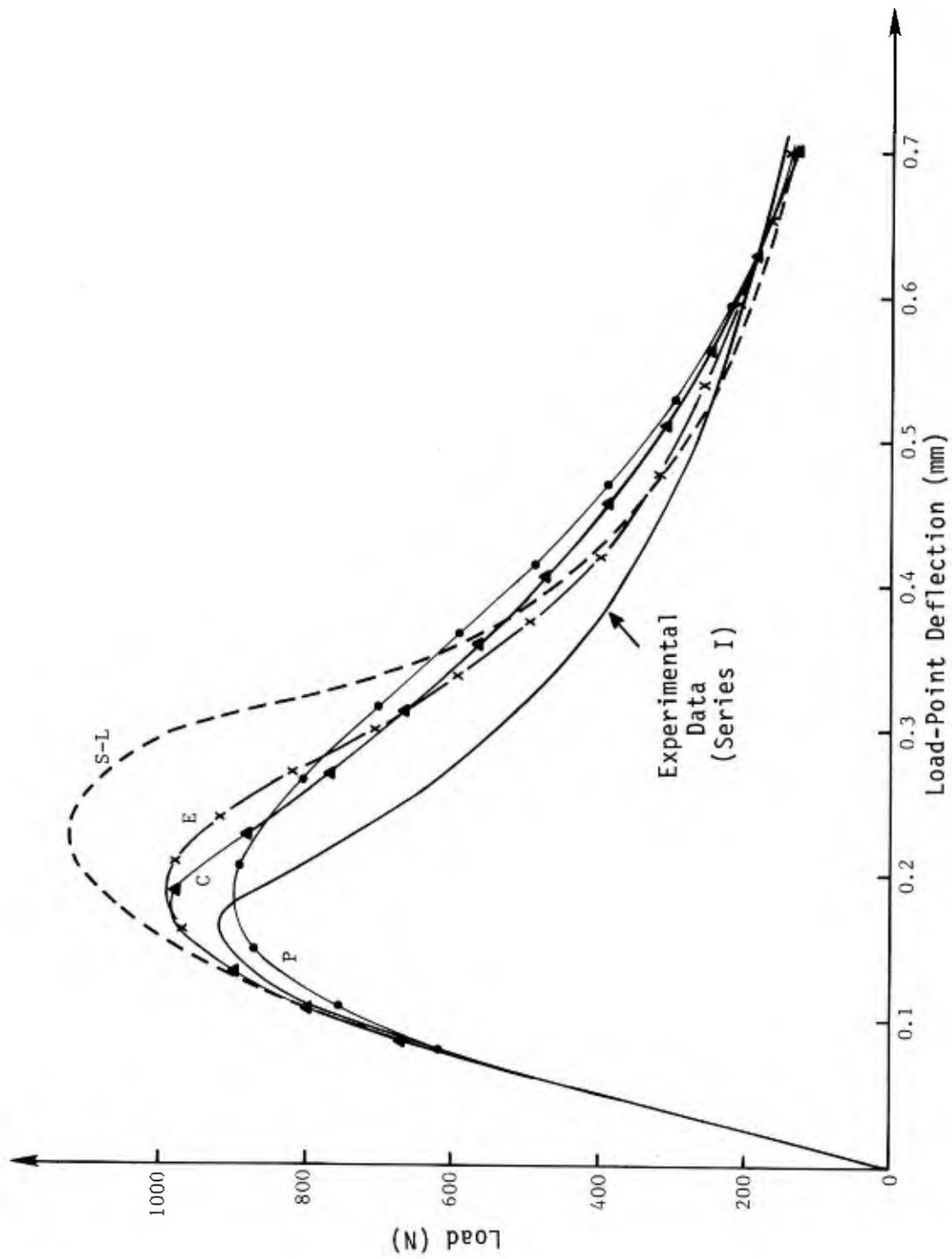| Group	a/W	Specimen	G_f (N/m)	$G_f^{\#}$ (N/m)	Peak load (N)	Unloading at (% of peak load)	d_p (mm)	d_o (mm)	Δa (mm)
		1	80.8	71.9	1683	88	0.13	3.3	4.2
		4	85.3	74.3	2133	93	0.16	2.1	7.6
1	0.3	7	69.0	–	1951	–	0.15	2.3	–
		10	74.2	–	2200	–	0.15	1.9	–
–		Mean	77.3	73.1	1992	90	0.15	2.4	5.9
		2	58.9	–	1024	–	0.14	2.5	–
		5	76.9	68.9	1078	88	0.14	2.5	5.8
2	0.5	8	60.8	54.8	1127	87	0.13	2.1	6.1
		11	62.7	54.6	1140	97	0.15	2.0	0.7
–		Mean	64.8	59.4	1092	91	0.14	2.3	4.2
		3	44.9	44.4	410	96	0.16	1.8	5.5
		6	43.8	–	432		0.16	1.5	–
3	0.7	9	62.5	–	468	–	0.15	2.7	–
		12	43.6	40.8	330	93	0.15	1.9	3.6
–		Mean	48.7	42.6	410	94	0.15	2.0	4.5

Figure 9. Analytical representations.

Table 4. Results - Series III

N (mm)	Specimen	G_f (N/m)	$G_f^{\#}$ (N/m)	Peak load (N)	Unloading at (% of peak load)	d_p (mm)	d_o (mm)	Δa (mm)
	1	76.6	76.8	909	90	0.14	2.9	7.9
	3	81.9	-	958	-	0.16	2.9	-
102	5	71.6	70.6	908	89	0.15	2.9	7.9
	7	59.2	58.2	793	92	0.12	3.0	3.2
—	Mean	72.3	68.5	892	90	0.14	2.9	6.3
	2	84.7	-	3795	-	0.09	1.9	-
	5	89.5	-	3900	-	0.10	2.2	-
216	8	90.7	-	3875	-	0.11	1.9	-
	11	92.2	85.7	3580	89	0.10	2.0	7.2
—	Mean	89.3	85.7	3788	89	0.10	2.0	7.2

Sensitivity analyses (Ref 17) and further analyses by the authors have shown that the model is typically not as sensitive to variations in G_f as it is to variations of the other parameters. Most of the energy does appear to dissipate through crack surface formation ensuring the validity of the model.

G_f versus G_f^*

G_f^* was defined in an attempt to quantify and eliminate the energy dissipated outside of the crack zone. The strong variation of G_f with a_o/W seems to indicate a dependency on the stress field, i.e., an energy dissipation through microcracking in the process zone which is greater than indicated by G_f^*. For standard specimen sizes, the difference between G_f^* and G_f is about 5 percent while the fracture energy shows variations in the order of 25 percent. Furthermore, both values vary in the same manner and show size and geometry dependency. The proposed

approach does not seem to discard all the energy spent in the process zone. Further research is needed to refine the model. Given the additional steps involved in its evaluation, G_f^* does not appear to present any practical advantage over G_f.

Crack Front

The crack front appearance seems to be linked to the dye impregnation procedure. When the dye was inserted only from the top, the crack front appeared straight. In a few cases the dye was inserted from the sides and the top, and then the front appeared curved (Ref 16). The latter crack front appearance seemed to indicate an anisotropy of the process zone where the microcracks would tend to merge laterally before joining the macrocrack. In the determination of G_f^* a straight front was assumed.

Analytical Model

The good agreement between the ascending part of the LLPD curve of the average experimental plot and the model results supports the acceptability of using E from standard cylinder tests. This is an advantage since E is more readily available than E_d.

Among the different σ versus w relations, the SL is the coarsest, followed by the E and the P models. The bilinear relation, C, gives only a slight overestimation of the peak load and reasonably approaches the descending branch. Keeping f_t and G_f constant, the bilinear relationship could be improved to yield a better match, as done by Roelfstra and Wittmann (Ref 18) and Carpinteri et al. (Ref 19).

CONCLUSIONS AND RECOMMENDATIONS

The fracture for notched beams in three-point bending was experimentally determined. Three series of tests were conducted on a total of 32 beams and a finite element analysis carried out using a nonlinear model. The following conclusions were derived:

- The experimental setup led to more reliable and consistent values of concrete fracture energy and measured crack length.

- G_f^* (calculated by current crack size and ligament area) did not present any substantial advantage over G_f (determined by RILEM guidelines).

- Finite element analysis yielded accurate representations of the fracture behavior when coupled with a bilinear stress versus crack width relation.

- G_f is dependent upon size and geometry. The fracture energy increases with increasing size.

The inconsistency that arises from applying the FCM approach seems to be linked to its inability to represent the nonlinearity of the material and the energy dissipation outside the fracture zone. The model assumes all the energy to transform into surface energy through formation of a single major crack and only introduces nonlinearity in the stress-crack width relation.

The fracture model for plain concrete should be extended to three-dimensional applications and to bar-reinforced concrete. To add reinforcement, the mechanism for transferring shear from concrete to steel will need to be modeled, but the technological risk is low.

ACKNOWLEDGMENT

REFERENCES

1. A. Hillerborg, M. Modeer, and P.E. Peterson. "Analysis of crack formation and crack growth in concrete by means of fracture mechanics and finite elements," Cement and Concrete Research, vol 6, 1976, pp 773-782.

2. Y.R. Rashid. "Analysis of prestressed concrete pressure vessels," Nuclear Engineering and Design, vol 7, no. 4, 1968, pp 334-344.

3. Z.P. Bazant and L. Cedolin. "Blunt crack band propagation in finite element analysis," Journal of the Engineering Mechanics Division, American Society of Civil Engineers, vol 105, no. EM2, 1979, pp 297-315.

4. Z.P. Bazant and B.H. Oh. "Crack band theory for fracture of concrete," Materials and Structures, vol 16, no. 93, May-Jun 1983, pp 155-177.

5. Z.P. Bazant, J.K. Kim, and P. Pfeiffer. "Continuum model for progressive cracking and identification of nonlinear fracture parameters," Applications of Fracture Mechanics to Cementitious Composites (S.P. Shah, editor), NATO-ARW, Northwestern University, Dordrecht, The Netherlands, Sep 1984, pp 197-246.

6. Y. Jenq and S.P. Shah. "Two parameter fracture model for concrete," Journal of Engineering Mechanics, American Society of Civil Engineers, vol 111, no. 10, Oct 1985, pp 1227-1261.

7. RILEM Technical Committee 50-FMC. "Draft recommendation: Determination of the fracture energy of mortar and concrete by means of three-point bend tests on notched beams," Materials and Structures, no. 106, Jul-Aug 1985, pp 285-290.

8. S. Mindess. "Rate of loading effects on the fracture of cementitious materials," Applications of Fracture Mechanics to Cementitious Composites (S.P. Shah, editor), NATO-ARW, Northwestern University, Martinus Nijhoff publishers, Dordrecht, The Netherlands, Sep 1984, pp 617-636.

9. Kansas State University. Research Report 181: Evaluation of proposed methods to determine fracture parameters for concrete in bending, by S.E. Swartz and S.T. Yap. Manhattan, KS, Jun 1986.

10. ADINA Engineering Incorporated. ADINA: A finite element program for automatic dynamic incremental nonlinear analysis. Watertown, MA, Dec 1985.

11. Lund Institute of Technology. Report TVBM-1001: A fracture mechanics approach to failure analysis of concrete materials, by M.A. Modeer. Division of Building Materials, S-221 00, Lund, Sweden, 1979.

12. Lund institute of Technology. Report TVBM-1006: Crack growth and development of fracture zones in plain concrete and similar materials, by P.E. Peterson. Division of Building Materials, S-221 00, Lund, Sweden, 1981.

13. V.S. Gopalaratnam and S.P. Shah. "Softening response of plain concrete in direct tension," Journal of the American Concrete Institute, vol 82, no. 3, May-June 1985, pp 310-323.

14. P. Nallathambi and B.L. Karihaloo. "Prediction of load deflection behavior of plain concrete from fracture energy," Cement and Concrete Research, vol 16, 1986, pp 7-16.

15. H.W. Reinhardt. "Fracture mechanics of an elastic softening material like concrete," Delft University of Technology, The Netherlands, HERON, vol 29, no. 2, 1984, pp 1-42.

16. A. Bascoul, F. Kharchi, and J.C. Maso. "Concerning the measurement of the fracture energy of a micro-concrete according to the crack growth in a three point bending test on notched beams," Proceedings of the International Conference on Fracture of Concrete and Rock, Society for Experimental Mechanics, in Houston, Texas, June 1987, pp 631-643.

17. A. Hillerborg. "The theoretical basis of a method to determine the fracture energy of concrete," Materials and Structures, no. 106, Jul-Aug 1985, pp 291-296.

18. P.E. Roelfstra and F.H. Wittmann. "Numerical method to link strain softening with failure of concrete," in Proceedings of the International Conference on Fracture Mechanics of Concrete, Lausanne, Switzerland, Oct 1985, pp 163-175.

19. A. Carpinteri, G. Colombo, G. Ferrara, and G. Giuseppetti. "Numerical simulation of concrete fracture through a bilinear softening stress-crack opening displacement law," in Proceedings of the International Conference on Fracture of Concrete and Rock, Society for Experimental Mechanics, Houston, Texas, June 1987 pp, 178-191.

DISTRIBUTION LIST

AF 6550 CES/DEEE, Patrick AFB, FL
AFESC TST (Library), Tyndall AFB, FL
ARMY AMCSM-WS, Alexandria, VA; ERADCOM Tech Supp Dir (DELSD-L), Ft Monmouth, NJ
ARMY BELVOIR R&D CEN STRBE-AALO, Ft Belvoir, VA; STRBE-BLORE, Ft Belvoir, VA
ARMY CERL Library, Champaign, IL
ARMY CRREL Library, Hanover, NH
ARMY ENGR DIST Phila, Lib, Philadelphia, PA
ARMY MISSILE R&D CMD Ch, Docs, Sci Info Ctr, Arsenal, AL
ADMINSUPU PWO, Bahrain
BUREAU OF RECLAMATION D-1512 (GS DePuy), Denver, CO; Smoak, Denver, CO
CBC Library, Davisville, RI
CBU 411, OIC, Norfolk, VA
COGARD R&DC Library, Groton, CT
COMDT COGARD Library, Washington, DC
NAVRESCEN PE-PLS, Tampa, FL
DIA DB-6E1, Washington, DC; DB-6E2, Washington, DC; VP-TPO, Washington, DC
DIRSSP Tech Lib, Washington, DC
DNA STTI/TL, Washington, DC
DTIC Alexandria, VA
DTRCEN Code 4111, Bethesda, MD
FCTC LANT, PWO, Virginia Bch, VA
GIDEP OIC, Corona, CA
LIBRARY OF CONGRESS Sci & Tech Div, Washington, DC
MARCORBASE Code 4.01, Camp Pendleton, CA
NAS Code 163, Keflavik, Iceland; Miramar, Code 1821A, San Diego, CA; PWO (Code 182) Bermuda; PWO,
    Key West, FL; PWO, Sigonella, Italy
NATL BUREAU OF STANDARDS Bldg Mat Div (Mathey), Gaithersburg, MD
NAVCAMS SCE (Code N-7), Naples, Italy
NAVCOASTSYSCEN Tech Library, Panama City, FL
NAVCOMMSTA Code 401, Nea Makri, Greece
NAVEODTECHCEN Tech Library, Indian Head, MD
NAVFACENGCOM Code 03, Alexandria, VA; Code 04A, Alexandria, VA; Code 04A1D, Alexandria, VA;
    Code 04A3, Alexandria, VA; Code 04A4E (Bloom), Alexandria, VA; Code 04B2 (M. Yachnis),
    Alexandria, VA; Code 0631 (Cyphers), Alexandria, VA; Code 1002B, Alexandria, VA; Code 1113,
    Alexandria, VA
NAVFACENGCOM - CHES DIV. FPO-1PL, Washington, DC
NAVFACENGCOM - LANT DIV. Library, Norfolk, VA
NAVFACENGCOM - NORTH DIV. Code 04AL, Philadelphia, PA
NAVFACENGCOM - PAC DIV. Library, Pearl Harbor, HI
NAVFACENGCOM - SOUTH DIV. Library, Charleston, SC
NAVFACENGCOM - WEST DIV. Code 04A2.2 (Lib), San Bruno, CA
NAVFACENGCOM CONTRACTS OICC, Rota, Spain
ARMY CORPS OF ENGRS Library, Seattle, WA
NATL BUREAU OF STANDARDS R Chung, Gaithersburg, MD
NAVCHAPGRU Code 60, Williamsburg, VA
-1 Tech Lib, Pensacola, FL
NAVFACENGCOM Code 00, Alexandria, VA; Code 03T (Essoglou), Alexandria, VA; Code 04A1,
    Alexandria, VA; Code 07A (Herrmann), Alexandria, VA; Code 07M (Gross), Alexandria, VA; Code
    09M124 (Lib), Alexandria, VA
NAVFACENGCOM - LANT DIV. Br Ofc, Dir, Naples, Italy
NAVFACENGCOM CONTRACTS DROICC, Lemoore, CA; ROICC, Virginia Beach, VA
NAVOCEANSYSCEN DET, Tech Lib, Kailua, HI
NAVSHIPREPFAC Library, Guam
NAVSHIPYD Code 202.4, Long Beach, CA; Library, Portsmouth, NH
NAVSTA CO, Roosevelt Roads, PR; Engrg Dir, Rota, Spain
NAVSUPPACT PWO, Naples, Italy
NAVSUPPO Sec Offr, La Maddalena, Italy
NAVSWC Code E211 (Miller), Dahlgren, VA; Code W42 (R Ponzetto), Dahlgren, VA; PWO, Dahlgren, VA
NRL Code 5800, Washington, DC
OCNR DET, Code 481, Bay St. Louis, MS
PACMISRANFAC HI Area, PWO, Kekaha, HI
PERRY OCEAN ENGRG R. Pellen, Riviera Beach, FL
PMTC Code 1018, Point Mugu, CA

PWC ACE Office, Norfolk, VA; Code 101 (Library), Oakland, CA; Code 123-C, San Diego, CA; Code 420, Great Lakes, IL; Library (Code 134), Pearl Harbor, HI; Library, Guam, Mariana Islands; Library, Norfolk, VA; Library, Pensacola, FL; Library, Yokosuka, Japan; Tech Library, Subic Bay, RP
US DEPT OF INTERIOR Natl Park Svc, RMR/PC, Denver, CO
USS USS FULTON, Code W-3
CALIFORNIA Nav & Ocean Dev (Armstrong), Sacramento, CA
CLARKSON COLL OF TECH CE Dept (Batson), Potsdam, NY
COLORADO SCHOOL OF MINES Dept of Engrg (Chung), Golden, CO
COLORADO STATE UNIVERSITY CE Dept (W Charlie), Fort Collins, MD
CORNELL UNIVERSITY Civil & Environ Engrg (Dr. Kulhawy), Ithaca, NY; Library, Ithaca, NY
DUKE UNIVERSITY CE Dept (Muga), Durham, NC
FLORIDA ATLANTIC UNIVERSITY Ocean Engrg Dept (Hart), Boca Raton, FL; Ocean Engrg Dept (McAllister), Boca Raton, FL; Ocean Engrg Dept (Su), Boca Raton, FL
FLORIDA INST OF TECH CE Dept (Kalajian), Melbourne, FL; J Schwalbe, Melbourne, FL
JOHNS HOPKINS UNIV CE Dept (Jones), Baltimore, MD; Ches Bay Rsch Inst, Rsch Lib, Shady Side, MD
LAWRENCE LIVERMORE NATL LAB FJ Tokarz, Livermore, CA; L-654, Plant Engrg Lib, Livermore, CA
LEHIGH UNIVERSITY Linderman Library, Bethlehem, PA
MIT Engrg Lib, Cambridge, MA
NATL ACADEMY OF SCIENCES NRC, Naval Studies Bd, Washington, DC
OKLAHOMA STATE UNIV CE Scol (Lloyd), Stillwater, OK
PENNSYLVANIA STATE UNIVERSITY Applied Rsch Lab, State College, PA
PURDUE UNIVERSITY Engrg Lib, W. Lafayette, IN
STATE UNIVERSITY OF NEW YORK CE Dept, Buffalo, NY
TEXAS A&I UNIVERSITY Civil & Mech Engr Dept, Kingsville, TX
TEXAS A&M UNIVERSITY Ocean Engr Proj, College Station, TX
UNIV OF TENNESSEE CE Dept (Kane), Knoxville, TN
UNIVERSITY OF CALIFORNIA Engrg Lib., Berkeley, CA
UNIVERSITY OF DELAWARE CE Dept, Ocean Engrg (Dalrymple), Newark, DE; Engrg Col (Dexter), Lewes, DE
UNIVERSITY OF HAWAII Manoa, Library, Honolulu, HI
UNIVERSITY OF ILLINOIS Library, Urbana, IL; Metz Ref Rm, Urbana, IL
UNIVERSITY OF RHODE ISLAND CE Dept (Kovacs), Kingston, RI
UNIVERSITY OF TEXAS CE Dept (R Olson), Austin, TX; CE Dept (Thompson), Austin, TX
UNIVERSITY OF CALIFORNIA CE Dept (Fenves), Berkeley, CA
UNIVERSITY OF TEXAS ECJ 5.402 (Friedrich), Austin, TX
UNIVERSITY OF WASHINGTON CE Dept (N. Hawkins), Seattle, WA
WESTERN ARCHEOLOGICAL CEN Library, Tucson, AZ
AMERICAN SYS ENGRG CORP B. Williamson, Virginia Beach, VA
AMERICAN CONCRETE INSTITUTE Library, Detroit, MI
BATTELLE New Eng Marine Rsch Lab, Lib, Duxbury, MA
GOULD INC. Ches Instru Div, Tech Lib, Glen Burnie, MD
LINDA HALL LIBRARY Doc Dept, Kansas City, MO
NEW ZEALAND NZ Concrete Rsch Assoc, Library, Porirua
SEATECH CORP Peroni, Miami, FL
TIDEWATER CONSTR CO J Fowler, Virginia Beach, VA
TRW INC Engr Library, Cleveland, OH
WISS, JANNEY, ELSTNER, & ASSOC DW Pfeifer, Northbrook, IL
WOODWARD-CLYDE CONSULTANTS R Cross, Walnut Creek, CA
WESTCOTT, WM Miami, FL

INSTRUCTIONS

The Naval Civil Engineering Laboratory has revised its primary distribution lists. The bottom of the label on the reverse side has several numbers listed. These numbers correspond to numbers assigned to the list of Subject Categories. Numbers on the label corresponding to those on the list indicate the subject category and type of documents you are presently receiving. If you are satisfied, throw this card away (or file it for later reference).

If you want to change what you are presently receiving:

- Delete — mark off number on bottom of label.
- Add — circle number on list.
- Remove my name from all your lists — check box on list.
- Change my address — line out incorrect line and write in correction (PLEASE ATTACH LABEL).
- Number of copies should be entered after the title of the subject categories you select.

Fold on line below and drop in the mail.

Note: Numbers on label but not listed on questionnaire are for NCEL use only, please ignore them.

Fold on line and staple.

DEPARTMENT OF THE NAVY

NAVAL CIVIL ENGINEERING LABORATORY
PORT HUENEME, CALIFORNIA 93043-5003

OFFICIAL BUSINESS
PENALTY FOR PRIVATE USE, $300
NCEL-2700/4 (REV. 10-87)
0930-LL-L70-0044

BUSINESS REPLY CARD

FIRST CLASS   PERMIT NO. 69

POSTAGE WILL BE PAID BY ADDRESSEE

Commanding Officer
Code L08B
Naval Civil Engineering Laboratory
Port Hueneme, California 93043-5003

NO POSTAGE
NECESSARY
IF MAILED
IN THE
UNITED STATES

DISTRIBUTION QUESTIONNAIRE

The Naval Civil Engineering Laboratory is revising its primary distribution lists.

SUBJECT CATEGORIES

1 SHORE FACILITIES
2 Construction methods and materials (including corrosion control, coatings)
3 Waterfront structures (maintenance/deterioration control)
4 Utilities (including power conditioning)
5 Explosives safety
6 Aviation Engineering Test Facilities
7 Fire prevention and control
8 Antenna technology
9 Structural analysis and design (including numerical and computer techniques)
10 Protective construction (including hardened shelters, shock and vibration studies)
11 Soil/rock mechanics
14 Airfields and pavements

15 ADVANCED BASE AND AMPHIBIOUS FACILITIES
16 Base facilities (including shelters, power generation, water supplies)
17 Expedient roads/airfields/bridges
18 Amphibious operations (including breakwaters, wave forces)
19 Over-the-Beach operations (including containerization, materiel transfer, lighterage and cranes)
20 POL storage, transfer and distribution

28 ENERGY/POWER GENERATION
29 Thermal conservation (thermal engineering of buildings, HVAC systems, energy loss measurement, power generation)
30 Controls and electrical conservation (electrical systems, energy monitoring and control systems)
31 Fuel flexibility (liquid fuels, coal utilization, energy from solid waste)
32 Alternate energy source (geothermal power, photovoltaic power systems, solar systems, wind systems, energy storage systems)
33 Site data and systems integration (energy resource data, energy consumption data, integrating energy systems)
34 ENVIRONMENTAL PROTECTION
35 Solid waste management
36 Hazardous/toxic materials management
37 Wastewater management and sanitary engineering
38 Oil pollution removal and recovery
39 Air pollution
44 OCEAN ENGINEERING
45 Seafloor soils and foundations
46 Seafloor construction systems and operations (including diver and manipulator tools)
47 Undersea structures and materials
48 Anchors and moorings
49 Undersea power systems, electromechanical cables, and connectors
50 Pressure vessel facilities
51 Physical environment (including site surveying)
52 Ocean-based concrete structures
54 Undersea cable dynamics

TYPES OF DOCUMENTS

85 Techdata Sheets

86 Technical Reports and Technical Notes

83 Table of Contents & Index to TDS

82 NCEL Guides & Abstracts

91 Physical Security

[] None—
remove my name